ELSEVIER

Journal of Alloys and Compounds 330–332 (2002) 191–196

Journal of ALLOYS AND COMPOUNDS

www.elsevier.com/locate/jallcom

X-ray diffraction, neutron scattering and NMR studies of hydrides formed by Ti_4Pd_2O and Zr_4Pd_2O

J.S. Cantrell[a,*], R.C. Bowman Jr.[b], A.J. Maeland[c]

[a]*Chemistry and Biochemistry Department, Miami University, Oxford, OH 45056, USA*
[b]*Jet Propulsion Laboratory, California Institute of Technology, 4800 Oak Grove Drive, Pasadena, CA 91109, USA*
[c]*Department of Physics, Institute for Energy Technology, PO Box 40, N-2007 Kjeller, Norway*

Abstract

The oxygen-stabilized Ti_4Pd_2O and Zr_4Pd_2O alloys with the cubic $E9_3$-Ti_2Ni type structure have been reacted with hydrogen gas. Powder X-ray diffraction (XRD) has shown that the hydride phase retains a face-centered-cubic unit cell with an expansion of lattice parameter that is dependent on hydrogen content. The crystal structure has been solved for $Zr_4Pd_2OD_{3.5}$ by neutron diffraction. NMR measurements of proton relaxation times were made on $Ti_4Pd_2OH_{5.0}$ to assess diffusion behavior. Although the activation energy of 0.39 eV derived for $Ti_4Pd_2OH_{5.0}$ was nearly identical to the value found for hydrogen diffusion in oxygen-free $Ti_2PdH_{1.47}$, the spin-lattice (T_{1d}) and rotating-frame ($T_{1\rho}$) relaxation times minima were at much lower temperatures for $Ti_4Pd_2OH_{5.0}$, which implies more rapid hydrogen diffusion rates in the oxygen-stabilized phase. The nearest neighbor coordination sites that are involved in proposed hydrogen diffusion path ways are discussed and compared to the deuterium sites of $Zr_4Pd_2OD_{3.5}$.

Keywords: Metal hydrides; Crystal structure; Hydrogen diffusion; X-ray powder diffraction; Neutron powder diffraction; Nuclear magnetic resonance

1. Introduction

Numerous ternary oxide alloys have been prepared [1,2] with the Ti_2Ni-type $E9_3$ cubic (Fd3m)-structure (which is also commonly referred to as the η-carbide phase [3,4]). Many of the related $(Ti,Zr)_2M$ (M=Fe, Co, Ni, Cu, or Pd) binary alloys will react with hydrogen to form metastable ternary hydrides [5,6] or directly disproportionate [7–9] to form the hydrides TiH_2 or ZrH_2, and a different binary alloy such as ZrPd. However, ternary oxides with $E9_3$ structure form hydride phases that resist disproportionation [7–9] and can be repeatedly hydrided and dehydrided without degrading, making these materials more attractive for various hydrogen storage applications.

While Westlake [10,11] thoroughly described his predictions for hydrogen site occupancies in hydrides with the $E9_3$ structure, there have been relatively few crystal structure determinations [3,12] to confirm his analysis. Knowledge of hydrogen site occupancy in other compositions of these ternary oxides should provide useful insights on allowable maximum hydrogen storage capacities as well as hydrogen diffusion mechanisms in this family. Nuclear magnetic resonance (NMR) has been used previously to study hydrogen diffusion behavior in Ti_2CuH_x, Ti_2PdH_x, and Zr_2PdH_x phases [13,14] that are derived from tetragonal $MoSi_2$-type alloys [2]. Comparisons of hydrogen diffusion behavior in oxygen modified hydrides with the $E9_3$ structure should provide interesting new insights on the impact of host crystal structure and hydrogen site occupancy on the diffusion processes.

2. Experimental details

The ternary alloy oxide compounds Ti_4Pd_2O and Zr_4Pd_2O were prepared by arc melting very high purity (i.e. 99.95 at.%) metals, and using stoichiometric amounts of the corresponding oxide ZrO_2 or TiO_2 which was 99.9% pure (analytical reagent). The desired three component composition was achieved by arc melting the mixtures, cooling, crushing and remelting for five cycles while keeping the materials in an argon atmosphere dry box. Duplicate preparations were made and crushed and mixed until no inhomogeneities were found by microscopy or powder X-ray diffraction (XRD). The final preparation step was to degas the ternary oxide alloys at 873 K and 0.1

*Corresponding author. Tel.: +1-513-529-2834; fax: +1-513-529-2834.

E-mail address: cantrejs@muohio.edu (J.S. Cantrell).

0925-8388/02/$ – see front matter
PII: S0925-8388(01)01454-2

Table 1
Lattice parameters and relative volume expansion ($\Delta V/V_{alloy}$) for $Zr_4Pd_2OH(D)_x$ and $Ti_4Pd_2OH_x$ with the cubic $E9_3$-Ti_2Ni-type structure determined by powder X-ray diffraction (XRD) and neutron diffraction (ND)

Sample	a (nm)	V (nm^3)	$\Delta V/V_{alloy}$	Method	Data point in Fig. 2
Zr_4Pd_2O	1.2406(9)	1.9094 (8)	–	XRD	
$Zr_4Pd_2OD_{4.64}$	1.2793(9)	2.0936(8)	0.0965	XRD	1
Zr_4Pd_2O	1.2110(8)	1.7757(9)	–	ND	
$Zr_4Pd_2OD_{4.41}$	1.2494(9)	1.9503(8)	0.0982	ND	2
Zr_4Pd_2O	1.2110(7)	1.7757(7)	–	ND	
$Zr_4Pd_2OD_{3.5}$	1.2620(7)	2.0099(6)	0.0824	ND	3
Zr_4Pd_2O	1.2458(9)	1.9335(8)	–	XRD (Ref. [8])	
Ti_4Pd_2O	1.207(5)	1.758(7)	–	XRD	
$Ti_4Pd_2OH_{5.0}$	1.245(9)	1.928(9)	0.0967	XRD	5

mPa. The change in weight was negligible for the arc melting and heat treatments of these ternary alloys.

The alloys were hydrided (or deuterided) at room temperature until constant pressure was obtained. Samples were cycled with hydrogen (or deuterium) to obtain homogeneous samples. No disproportionation into TiH_x or ZrH_x was observed and the samples were found to be homogeneous. Table 1 shows the hydrogen (deuterium) contents for several of these preparations along with their cubic (a) lattice parameters determined by either XRD or neutron diffraction. After producing the hydrides given in Table 1, the reaction vessels were opened in a glove box containing highly purified and recycled argon. Samples of the hydrided powders were taken for subsequent X-ray diffraction measurements using procedures described elsewhere [15]. The neutron diffraction measurements of $Zr_4Pd_2OD_x$ powder were performed and analyzed using procedures described previously [16].

A transient NMR spectrometer [13,14] was used to determine the proton spin-lattice (T_1) and rotating-frame ($T_{1\rho}$) relaxation times. The primary proton resonance frequency was 34.5 MHz, but some measurements were also made at 12.5 and 60.0 MHz. The spin-locking magnetic field for the $T_{1\rho}$ relaxation times was 7.3 G. The magnetization recoveries during the T_1 measurements were exponential as expected for protons in a single-phase host. However, the $T_{1\rho}$ recoveries were usually non-exponential as found previously for Ti_2CuH_x and Ti_2PdH_x samples [13,14]. Consequently, the $T_{1\rho}$ values are defined as the time for the decay to reach $1/e$ of its initial amplitude.

3. Results and discussion

The powder XRD pattern of the $Ti_4Pd_2OH_{5.0}$ hydride is shown in Fig. 1 where all the peaks above background have been indexed to the cubic $E9_3$-Ti_2Ni type structure with the lattice parameter $a=1.2232(2)$ nm. No peaks from impurity phases are seen in this pattern. The sharp, narrow diffraction peaks and absence of impurity phases indicate that the preparation has produced a homogeneous ternary alloy and that the reaction with hydrogen has not resulted in any disproportionation reaction as also observed with other $E9_3$ ternary oxides [7–9]. The lattice parameters for the cubic phase in several $Zr_4Pd_2OH(D)_x$ samples obtained from XRD and neutron diffraction are also given in Table 1. The patterns for one of the Zr_4Pd_2O alloys and its hydrides (deuterides) also contained weak peaks due to ~1–2% of ZrO_2, which indicates an incomplete reaction and implies oxygen content <1.0 for these samples. However, there was no evidence for the disproportionation product ZrH_x from the $Zr_4Pd_2OH(D)_x$ samples which is consistent with the stability exhibited by other ternary $E9_3$ oxides [7,9]. Table 1 also shows that hydride formation leads to an expansion of the host unit cell ($\Delta V/V$). The dependence of this expansion on hydrogen (deuterium) content for the samples in Table 1 and hydrides formed by other $E9_3$ oxides [4,8,17,18] is shown in Fig. 2. While the data show some scatter, there is an approximately linear expansion falling close to the line derived from Westlake's [10,11] prediction of a volume increase of 0.00257 nm^3 per hydrogen atom in this structure. The $\Delta V/V$ values for the four hydrides from Table 1 do not show much deviation from this line. Small uncertainities in alloy stoichiometry and hydrogen contents are primarily responsible. Much of the variation in $\Delta V/V$ for the hydrides of

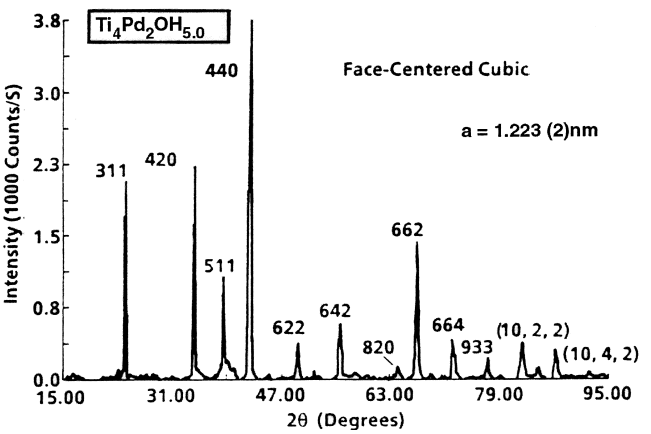

Fig. 1. The XRD profile for $Ti_4Pd_2OH_{5.0}$ where all the indexed peaks correspond to the Ti_2Ni-type $E9_3$ cubic structure.

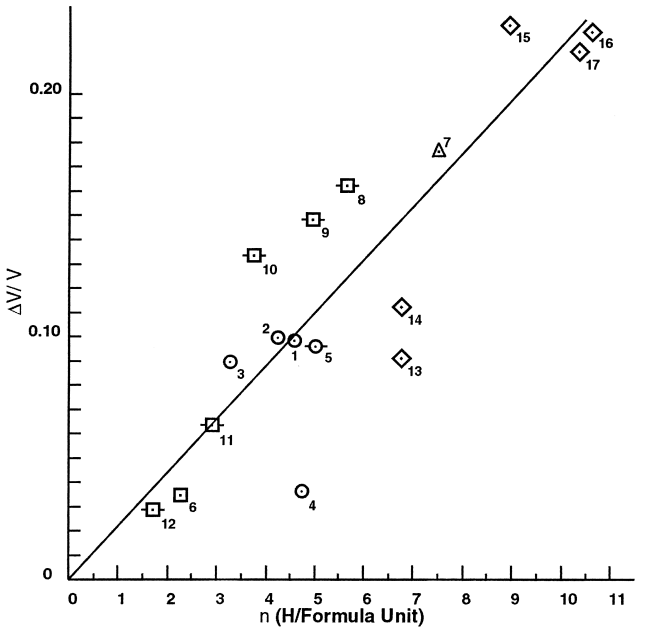

Fig. 2. The volume expansion for hydride phases of several ternary oxides ($Zr_4Pd_2OH(D)_x$: points 1–3, present work; $Zr_4Pd_2OH_{4.7}$: point 4, Ref. [8]; $Ti_4Pd_2OH_{5.0}$: point 5, present work; $Ti_4Fe_2O_yH_x$: point 6, 8–12, Refs. [11,17]; $Zr_4Fe_2O_{0.6}H_{7.5}$: point 7, Ref. [18]; $Zr_3Fe_3OD_x$: points 13–17, Ref. [4]) derived from XRD and neutron diffraction. The line is based upon a prediction by Westlake [10,11].

$Ti_4Fe_2O_y$, $Zr_4Fe_2O_{0.6}$ and Zr_3Fe_3O can be attributed to differences in the distributions of the H (D) atoms amongst the several available sites [10,11] in the $E9_3$ structure for these ternary oxides [12]. Zavaliy et al. [4,12,18] has shown recently that reducing the oxygen content in the $Zr_3V_3O_y$ and $Zr_4Fe_2O_y$ alloys ($0.2<y<1.0$) leads to significantly larger hydrogen storage with occupancy of additional types of sites. There is no reason to expect identical volume expansions for the hydrides of these ternary alloys as different types of sites are being filled. The low $\Delta V/V=0.0346$ for $Zr_4Pd_2OH_{4.7}$ previously reported by Maeland [8] is probably anomalous due to the lost of hydrogen and the actual hydrogen content was probably only ~2. The hydrogen content for this sample had not been determined after the XRD measurement.

Powder neutron diffraction measurements were performed on a $Zr_4Pd_2OD_{3.5}$ sample to solve its crystal structure and determine locations of the deuterium (hydrogen) sites in the interstices of the $E9_3$ phase. The structural parameters summarized in Table 2 were obtaining from a Rietveld refinement program [16] using neutron scattering lengths of $b(Zr)=0.716\times10^{-12}$ cm, $b(Pd)=0.591\times10^{-12}$ cm, and $b(D)=0.667\times10^{-12}$ cm. The neutron wavelength was 0.18250 nm and the cubic cell lattice parameter for the deuteride is 1.2620(8) nm. The Rietveld refinement proceeded to an R-factor = 0.02 with no significant differences from the Bragg diffraction peaks. Deuterium was found to be distributed over the interstitial sites designated D2, D4, and D7 by Westlake [10] with respective coordination Zr_3Pd_1, Zr_2Pd_2, and Zr_6. While these sites are occupied in the deuteride phases of other $E9_3$ ternary oxides [3,10–12], the combination is not identical to that obtained for $Zr_4Pd_2OD_{3.5}$. Differences in relative dimensions of the lattice parameters and host metal atomic radii strongly influence [10,11] which interstices are occupied by H(D).

To assess hydrogen diffusion behavior in the $Ti_4Pd_2OH_{5.0}$ sample, proton relaxation times were measured between 100 and 520 K. Some of these T_1 and $T_{1\rho}$ relaxation times are compared to values obtained for two Ti_2PdH_x samples under identical conditions in Figs. 3 and 4, respectively. The T_1 relaxation times in Fig. 3 for

Table 2
Profile refinement of the crystal structure for $Zr_4Pd_2OD_{3.5}$ from its neutron diffraction pattern

Atom	Position	x	y	z	n	Occupancy	Temperature factor
Zr1	48f	0.184	0	0	48	1.0	1.0
Zr2	16d	0.625	0.625	0.625	16	1.0	1.0
Pd	32e	0.918	0.918	0.918	32	1.0	1.0
O	16c	0.125	0.125	0.125	16	1.0	1.0
D2	192i	0.742	0.867	0.986	36	0.188	1.1
D4	96g	0.967	0.967	0.651	12	0.125	1.1
D7	8a	0	0	0	8	1.0	1.1

D-site locations in $Zr_4Pd_2OD_{3.5}$

Deuterium site	Wyckoff notation	Coordination	Occupation
D1	32e	Zr_3Pd_1	0
D2	192i	Zr_3Pd_1	0.188
D3	$96g_1$	$Zr_2Pd_1O_1$	0
D4	$96g_2$	Zr_2Pd_2	0.125
D5	8b	Pd_4	0
D6	32e	Zr_1Pd_3	0
D7	8a	Zr_6	1.0

Space group, $Fd3m$–O_h^7; wavelength (nm), 0.18250; lattice parameter, a (nm) = 1.2620(8); unit cell volume (nm^3), 2.0099(9).

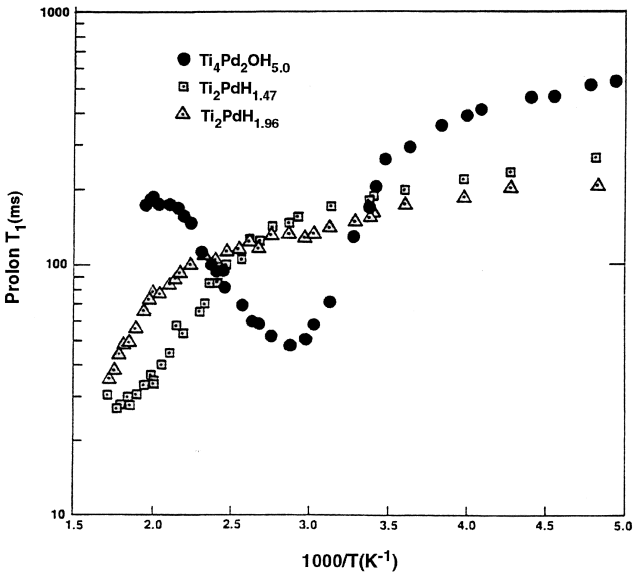

Fig. 3. Proton spin-lattice (T_1) relaxation times for $Ti_4Pd_2OH_{5.0}$, $Ti_2PdH_{1.47}$, and $Ti_2PdH_{1.96}$ measured at resonance frequency of 34.5 MHz.

$Ti_4Pd_2OH_{5.0}$ can be separated into the expected [19] Korringa conduction electron interaction (T_{1e}) with $T_{1e}T=$ 105.0 sK and the diffusion dependent dipolar relaxation time T_{1d}. When the well-known BPP (Bloembergen-Purcell-Pound) model [19] is used to determine the proton diffusion correlation times from these T_{1d} data, an activation energy (E_a) of 0.39 eV is obtained. A prominent feature in Fig. 3 is the well-defined T_1 minimum at 350 K for $Ti_4Pd_2OH_{5.0}$ while this minimum is barely observed (or not yet reached) until $T>550$ K for the Ti_2PdH_x samples. The minima in the T_{1d} and $T_{1\rho}$ relaxation times are definitive signatures [19] of diffusion dominance that furthermore obey the relations $\tau_d^{-1}=\omega_0/0.70$ and $\tau_\rho^{-1}=\omega_1/0.57$, respectively, [20] where τ_d is the mean dwell time of the H atom in an interstitial site, ω_0 is the resonance Larmor frequency, and ω_1 is the rotating-frame frequency. Hence, the proton mobility in $Ti_4Pd_2OH_{5.0}$ is much faster than in the Ti_2PdH_x samples. This behavior is verified by the $T_{1\rho}$ times presented in Fig. 4 as well as diffusion correlation times in Fig. 5 that were derived from these data using the BPP model. The resulting diffusion E_a values from these plots along with the corresponding temperature (T_{min}) of the T_{1d} and $T_{1\rho}$ minima are summarized in Table 3. Also included in this table are similar diffusion parameters for several other Ti-based hydrides [13,14,20–25] and $PdH_{0.73}$ [26]. We recognize that recent studies [19,27] have shown the E_a values obtained using the BPP model tend to be ~10–15% too small compared to results from lattice-specific models or direct pulsed-field gradient diffusion coefficient measurements. However, the necessary lattice sums [19] required to perform these more precise relaxation time analyses are not available and are

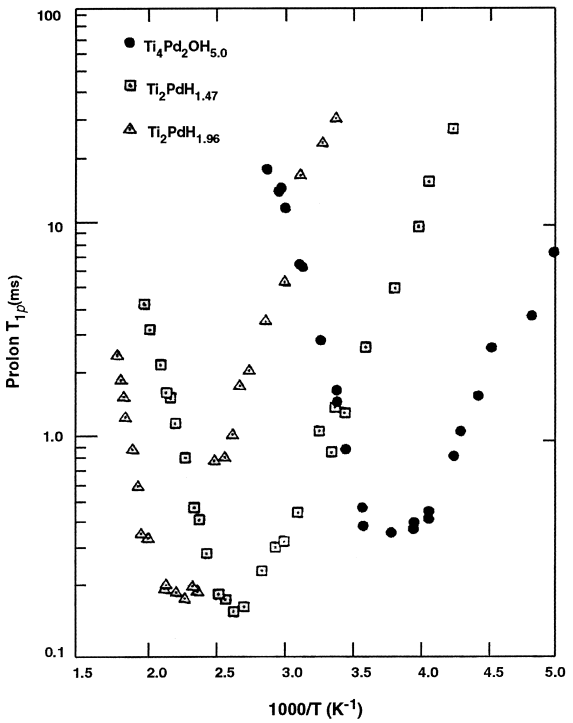

Fig. 4. Proton rotating frame relaxation times $Ti_4Pd_2OH_{5.0}$, $Ti_2PdH_{1.47}$, and $Ti_2PdH_{1.96}$.

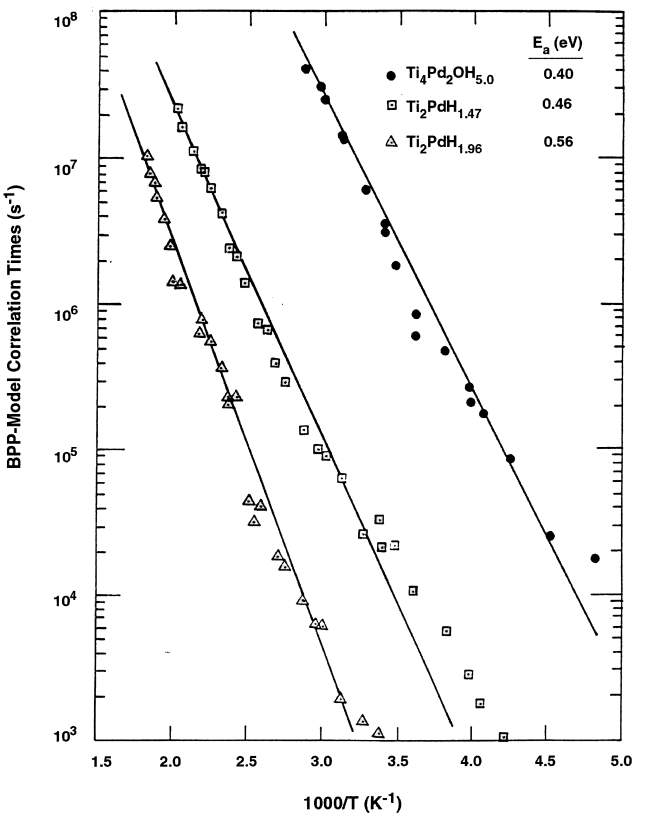

Fig. 5. Diffusion correlation times from BPP model analyses of the rotating frame relaxation times in Fig. 4.

Table 3
Hydrogen diffusion parameters for Ti-based hydrides from proton NMR relaxation time T_{1d} and $T_{1\rho}$ (includes host structure and hydrogen site occupancy)

Hydride	Hydride structure (type)	H-site occupancy	Relaxation time	ω (rad/s)	T_{min} (K)	E_a (eV)	Data sources
$Ti_4Pd_2OH_{5.0}$	f.c.c. ($E9_3$-Ti_2Ni)	Ti_3Pd_1(D2), Ti_3Pd_1(D4), Ti_6(D7)[a]	T_{1d} T_{1d} T_{1d} $T_{1\rho}$	0.79×10^8 2.17×10^8 3.77×10^8 1.95×10^5	331 350 357 260	0.37 0.39 0.43 0.40	Present work
$TiH_{1.95}$	f.c.c. (CaF_2)	Ti_4	$T_{1\rho}$	1.95×10^5	455	0.50	Present work
$TiH_{1.90}$	f.c.c. (CaF_2)	Ti_4	T_{1d} $T_{1\rho}$	1.19×10^8 4.12×10^5	640 ~425	0.51 0.51	Ref. [21] Ref. [22]
$Ti_2PdH_{1.47}$	Orthorhombic (from $MoSi_2$)	Ti_4	T_{1d} $T_{1\rho}$	2.17×10^8 1.95×10^5	550 374	0.40 0.46	Ref. [14]
$Ti_2PdH_{1.96}$	Orthorhombic (from $MoSi_2$)	Ti_4	T_{1d} $T_{1\rho}$	2.17×10^8 1.95×10^5	>580 431	0.54 0.55	Ref. [14]
$Ti_2CuH_{1.9}$	Tetragonal ($MoSi_2$)	Ti_4	$T_{1\rho}$	1.95×10^5	424	0.40	Refs. [5,13,16]
$Ti_2CuH_{2.63}$	Orthorhombic (from $MoSi_2$)	Ti_4, Ti_4Cu_2	$T_{1\rho}$	1.95×10^5	470	0.64	Refs. [5,13,16]
$TiCuH_{0.94}$	b.c.t.	Ti_4	$T_{1\rho}$	1.95×10^5	483	0.87	Ref. [13]
$TiCr_{1.8}H_{2.58}$	f.c.c. (C15-$MgCu_2$)	Ti_2Cr_2 (g-sites)	T_{1d} $T_{1\rho}$	2.17×10^8 1.95×10^5	240 169	0.14 0.25	Ref. [23]
$TiCr_{1.9}H_{2.85}$	Hexagonal (C14-$MgZn_2$)	Ti_2Cr_2	T_{1d} $T_{1\rho}$	2.17×10^8 1.95×10^5	255 184	0.28 0.40	Ref. [23]
$ZrTi_2H_{3.9}$	f.c.c. (C15-$MgCu_2$)	$ZrTi_3$, (Zr_2Ti_2) (e-sites and g-sites)	T_{1d} $T_{1\rho}$	1.21×10^8 2.76×10^5	262 163	0.22/0.11 0.22	Ref. [20]
$Ti_{0.8}V_{0.2}H_{0.89}$	b.c.c.	$Ti_{4-y}V_y$(91%), V_6(9%)	T_{1d}	5.65×10^7	217	0.25	Refs. [24,25]
$Ti_{0.6}V_{0.4}H_{0.91}$	b.c.c.	$Ti_{4-y}V_y$(81%), V_6(19%)	T_{1d}	5.65×10^7	215	0.24	Refs. [24,25]
$Ti_{0.4}V_{0.6}H_{0.91}$	b.c.c.	$Ti_{4-y}V_y$(64%), V_6(36%)	T_{1d}	5.65×10^7	200	0.23	Refs. [24,25]
$PdH_{0.73}$	f.c.c. (NaCl)	Pd_6	T_{1d} $T_{1\rho}$	3.52×10^8 0.27×10^5	~285 <170	0.23 0.23	Ref. [26]

[a] Based upon deuterium locations from present structure determination for $Zr_4Pd_2OD_{3.5}$.

extremely difficult to generate in complex structures and when hydrogen occupies several different sites. Hence, the BPP-based E_a values in Table 3 will provide a convenient and practical approach to discuss the general impacts of host structure and H site symmetry on hydrogen mobility.

A very wide range of hydrogen mobility for the different Ti-based hydrides is indicated by the variation in E_a and T_{min} values in Table 3. Diffusion rates will increase dramatically for lower activation energies and lead to decreases in the minimum temperatures for the relaxation times. As discussed previously [13–15], host structure and metal coordination at the H sites greatly impact the diffusion rate. The close proximity of vacant available sites, as found in the C14 and C15 AB_2H_x Laves phases, permits extremely rapid localized motion [20,23] and very fast long-range diffusion. Similar short separations between the tetrahedral interstices (as well as occupancy of octahedral sites) account for the fast diffusion in the b.c.c. $Ti_{1-y}V_yH_{0.9}$ phases [24,25]. In contrast, large barriers to diffusion can arise from layers of poor bonding metals (e.g. Cu) resulting in larger E_a values and increases in T_{min} for $T_{1\rho}$ between TiH_x and $TiCuH_{0.94}$ [22,23]. The diffusion parameters for hydrides formed by the $MoSi_2$-type alloys [13,14] are very similar to f.c.c. TiH_x [21,22,27] when only the Ti_4 sites are occupied. The presumed occupancy of several sites in $Ti_4Pd_2OH_{5.0}$, based upon the present structure determination for $Zr_4Pd_2OD_{3.5}$ and previous studies on hydrides of other $E9_3$ oxides [3,10–12], is the likely cause for the greater hydrogen mobility in this hydride. However, the relaxation times in Figs. 3 and 4 do not show the anomalous temperature and frequency behavior that is ascribed to rapid localized motion in the AB_2 Laves phases [23,28]. It is more likely that occupancy of the octahedral Ti_6 sites in $Ti_4Pd_2OH_{5.0}$ permit more rapid long-range diffusion without involving some fraction of the protons in highly localized motions. Further structural information and more extensive diffusion studies are needed to describe the relevant mechanisms.

4. Conclusions

The cubic oxygen-stabilized Ti_4Pd_2O and Zr_4Pd_2O alloys form stable hydrides with expanded unit cells that correlate well with other $E9_3$ ternary oxides. Based upon the structure of a $Zr_4Pd_2OD_{3.5}$ sample, three distinct interstitial sites are occupied by D(H). The hydrogen mobility in $Ti_4Pd_2OH_{5.0}$ is much more rapid than for TiH_x or ternary hydrides formed by alloys with the $MoSi_2$ structure. However, the diffusion rate is much smaller than found for Ti-based hydride with the b.c.c. or Laves structures. The hydrides of these oxides are excellent candidates for more in-depth examination of the roles of host structure and multiple H site occupancy on hydrogen diffusion mechanisms.

Acknowledgements

This research was partially supported by the Jet Propulsion Laboratory, California Institute of Technology, under a contract with the National Aeronautical and Space Administration. The authors thank Drs A. Attalla and G.C. Abell for their assistance with the NMR experiments and analyses.

References

[1] M.V. Nevitt, J.W. Downey, R.A. Morris, Trans. Met. Soc. AIME 218 (1960) 1019.
[2] M.V. Nevitt, in: J.H. Westbrook (Ed.), Intermetallic Compounds, Wiley, New York, 1967, p. 214.
[3] F.J. Rotella, H.E. Flotow, D.M. Gruen, J.D. Jorgensen, J. Chem. Phys. 79 (1983) 4522.
[4] I.Y. Zavaliy, J. Alloys Comp. 291 (1999) 102.
[5] R.J. Furlan, G. Bambakidis, J.S. Cantrell, R.C. Bowman Jr., A.J. Maeland, J. Less-Common Met. 116 (1986) 375.
[6] J.S. Cantrell, R.C. Bowman Jr., J. Less-Common Met. 172–174 (1991) 29.
[7] M.H. Mintz, Z. Hadari, M.P. Dariel, J. Less-Common Met. 74 (1980) 287.
[8] A.J. Maeland, J. Less-Common Met. 89 (1983) 173.
[9] H.T. Takeshita, H. Tanaka, N. Kuriyama, T. Sakai, I. Uehara, M. Haruta, J. Alloys Comp. 298 (2000) 114.
[10] D.G. Westlake, J. Chem. Phys. 79 (1983) 4532.
[11] D.G. Westlake, J. Less-Common Met. 105 (1985) 69.
[12] I.Y. Zavaliy, W.B. Yelon, P.Y. Zavalij, I.V. Saldan, V.K. Pecharsky, J. Alloys Comp. 309 (2000) 75.
[13] R.C. Bowman Jr., A.J. Maeland, W.-K. Rhim, Phys. Rev. B 26 (1982) 6382.
[14] R.C. Bowman Jr., A. Attalla, G.C. Abell, J.S. Cantrell, A.J. Maeland, J. Less-Common Met. 172–174 (1991) 643.
[15] R.C. Bowman Jr., J.S. Cantrell, A.J. Maeland, A. Attalla, G.C. Abell, J. Alloys Comp. 185 (1992) 7.
[16] A.F. Andresen, A.J. Maeland, J. Less-Common Met. 129 (1987) 115.
[17] K. Hiebl, E. Tuscher, H. Bittner, Monatsh. Chem. 110 (1979) 9.
[18] I.Y. Zavaliy, A.B. Riabov, V.A. Yartys, G. Wiesinger, H. Michor, G. Hilscher, J. Alloys Comp. 265 (1998) 6.
[19] R.G. Barnes, in: H. Wipf (Ed.), Hydrogen in Metals III, Springer, Berlin, 1997, p. 93.
[20] A.V. Skripov, S.V. Rychkova, M.Y. Belyaev, A.P. Stepanov, Solid State Commun. 71 (1989) 1119.
[21] C. Korn, D. Zamir, J. Phys. Chem. Solids 31 (1970) 489.
[22] C. Korn, S.D. Goren, Phys. Rev. B 22 (1980) 4727.
[23] R.C. Bowman Jr., B.D. Craft, A. Attalla, J.R. Johnson, Int. J. Hydrogen Energy 8 (1983) 801.
[24] T. Ueda, S. Hayashi, J. Alloys Comp. 231 (1995) 226.
[25] T. Ueda, S. Hayashi, Y. Nakai, S. Ikeda, Phys. Rev. B 51 (1995) 5725.
[26] R.R. Arons, H.G. Bohn, H. Luetgemier, Solid State Commun. 14 (1974) 1203.
[27] U. Kaess, G. Majer, M. Stoll, D.T. Peterson, R.G. Barnes, J. Alloys Comp. 259 (1997) 74.
[28] A.V. Skripov, J. Combet, H. Grimm, R. Hempelmann, V.N. Kozhanov, J. Phys. Condens. Matter 12 (2000) 3313.